Bulletin of Mathematical Biology (2008) 70: 1994–2016
DOI 10.1007/s11538-008-9336-z

ORIGINAL ARTICLE

A PDE Model for Imatinib-Treated Chronic Myelogenous Leukemia

Peter S. Kim[a], Peter P. Lee[b], Doron Levy[c,*]

[a] *Laboratoire des Signaux et Systèmes, École Supérieure d'Électricité, 91192 Gif-sur-Yvette, France*
[b] *Division of Hematology, Department of Medicine, Stanford University, Stanford, CA 94305, USA*
[c] *Department of Mathematics and Center for Scientific Computation and Mathematical Modeling (CSCAMM), University of Maryland, College Park, MD 20742, USA*

Received: 4 February 2008 / Accepted: 29 April 2008 / Published online: 29 July 2008

Abstract We derive a model for describing the dynamics of imatinib-treated chronic myelogenous leukemia (CML). This model is a continuous extension of the agent-based CML model of Roeder et al. (Nat. Med. 12(10), 1181–1184, 2006) and of its recent formulation as a system of difference equations (Kim et al. in Bull. Math. Biol. 70(3), 728–744, 2008). The new model is formulated as a system of partial differential equations that describe various stages of differentiation and maturation of normal hematopoietic cells and of leukemic cells.

An imatinib treatment is also incorporated into the model. The simulations of the new PDE model are shown to qualitatively agree with the results that were obtained with the discrete-time (difference equation and agent-based) models. At the same time, for a quantitative agreement, it is necessary to adjust the values of certain parameters, such as the rates of imatinib-induced inhibition and degradation.

Keywords Chronic myelogenous leukemia · Gleevec · Imatinib · Mathematical models · Agent-based models · Difference equations · Partial differential equations

1. Introduction

Chronic Myelogenous Leukemia (CML) is a cancer that results in the overproduction of white blood cells. It represents nearly 20% of all leukemias and affects approximately 1 in 100,000 people. More than 90% of all CML cases are associated with the Philadelphia (Ph) chromosome, a genetic abnormality caused by a reciprocal translocation between chromosomes 9 and 22 (Thijsen et al., 1999). The recently developed, molecular targeted

*Corresponding author.
E-mail address: dlevy@math.umd.edu (Doron Levy).

drug imatinib has proven to be a highly effective treatment against CML (Druker and Lydon, 2000). While imatinib does not cure CML, it provides for most patients an effective mean of controlling CML expansion without resorting to more aggressive treatments such as chemotherapy or stem-cell transplantation (Campbell et al., 2001).

In recent years, there has been an ongoing activity in deriving mathematical models of CML. These works were motivated by the desire to explore the mechanisms that control the disease with the hope that this will lead, e.g., to new therapeutical strategies. We briefly mention a few and refer to the references therein for a complete picture. The first mathematical CML model is due to Fokas et al. (1991). A model that accounts for the immune response in CML is due to Neiman (2002). This work attempted to explain the transition of leukemia from the stable chronic phase to the erratic accelerated and acute phases. A more recent work is of Moore and Li (2004), whose aim was to identify the parameters that control cancer remission. Their main conclusion was that lower growth rates lead to a greater chance of cancer elimination. Komarova et al. used methods of stochastic networks to study drug resistance with a particular view toward imatinib (Komarova and Wodarz, 2005). Together with deConde, we have published in DeConde et al. (2005) a model for the interaction between the immune system and cancer cells after a stem cell (or a bone-marrow) transplant. The main result of that work was that a slightly elevated autologous (pretransplant) immune response greatly favors remission. Hence, mini-transplants may increase the chances of a full remission when compared with full allogeneic transplants. These ideas were further developed in Kim et al. (2007).

Recently, two models of stem cell differentiation and imatinib treatment have been proposed by Michor et al. (2005) and by Roeder et al. (2006). Michor et al. developed a differential equations model, in which leukemia cells progressively differentiate from stem cells to terminally differentiated cells (Michor et al., 2005). By comparing their model to patient data measured up to 450 days after the start of treatment, they concluded that leukemic stem cells are largely immune to imatinib. On the other hand, Roeder et al. proposed an agent-based model in which stem cells circulate between proliferating and quiescent states. The data set considered by Roeder et al. shows a sustained leukemia remission for at least 4 years. Consequently, the conclusion of that work is that imatinib can affect proliferating stem cells.

The different point of views were further stressed in a recent review paper by Abbott and Michor (2006). There, the conclusion that imatinib does not affect stem cells is reasserted. In a related work, Dingli and Michor (2006) derive a modified model of cell differentiation that is structurally similar to the original model in Michor et al. (2005). The analysis of this modified model lead them to conclude that an effective therapy to prevent a future relapse must target cancer stem cells. Hence, it still remains an important question to what degree imatinib affects leukemia stem cells.

Offering yet another perspective, Roeder and Glauche study the same issue in a review paper where they clearly point out that recently collected patient data indicates that imatinib-induced remission is sustained for at least 4 years in nearly all cases (Roeder and Glauche, 2008). These observations in conjunction with their mathematical models lead them to conclude that imatinib must have a nontrivial effect on leukemic stem cells.

Both groups seem to agree that the current data does not provide sufficient grounds to eliminate either hypothesis and that it is very important to determine the impact, if any, of imatinib on stem cells.

In this paper, we revisit the agent-based model of Roeder et al. (2006). This is a stochastic agent-based model for studying the effect of imatinib on CML. This model accounts for the progression of normal and leukemia cells through three stages of the myeloid lineage: stem cells, precursor cells, and mature cells. Their agent-based formulation captures the inherent diversity of individual members of a large population and accounts for the probabilistic behavior of individual cells. However, to capture this level of complexity, the algorithm is computationally demanding.

To accelerate the computational time of the Roeder model, we have recently derived an analogous system of difference equations that captures the dynamics of the original model (Kim et al., 2008). Our approach consisted of grouping cells with similar state variables into clusters and treating each cluster as a collective agent. This reformulation of the model, reduces the number of agents in the model and can be implemented deterministically, which eliminates the need to generate huge numbers of random variables, and hence it is substantially more efficient than the original ABM.

The goal of the present work is to derive a system of partial differential equations (PDEs) that describes the Roeder model. Instead of keeping the original discretization of time, we assume that time is continuous, an assumption that leads us to a system of PDEs that is analogous to the original ABM. The system of PDEs presented in this paper is the continuous version of our system of difference equations (Kim et al., 2008).

A PDE model has several advantages over the stochastic ABM: The PDE model can be solved much faster than the stochastic ABM. Complexity issues limited the original ABM from Roeder et al. (2006) to population sizes that were about 10% of the real sizes. Such limitations do not exist with a PDE model as the number of variables is fixed and is independent of the number of cells. In addition, the PDE model has the advantage of providing a direct access to macroscopic quantities. Various quantities can now depend on densities and constants can be treated from a macroscopic point of view instead of keeping track over individual parameters that correspond to individual cells. In addition, since the biological processes occur in continuous time—such a representation is desirable also from a modeling perspective. Furthermore, more accurate estimates of the problem's parameters can potentially be obtained in a continuous model that captures the dynamics in time with better resolution.

The system of PDEs developed in this paper is an alternative to the system presented in Roeder (2003). In this work, Roeder formulates a system in which the population variables are functions of time, t, and a state variable, a. Despite the simplicity of this system, numerical difficulties arise from an accumulation point in one of the populations at $a = 1$. At this point, the population density blows up in finite time. Various strategies can be considered for treating this problem, in particular, distributing the point mass at $a = 1$ over a small interval around $a = 1$. This is in fact the approach adopted in Roeder (2003).

The adjustment makes the system numerically solvable, but does not eliminate the numerical difficulties that arise from the huge difference in population densities inside and outside the interval around the point mass. Indeed, the difference between orders of magnitude can be arbitrarily large depending on how small one makes the interval. Alternatively, in our PDE system, we introduce a new population variable corresponding to the point mass at $a = 1$. In this fashion, we eliminate the difficulties that result from having an accumulation point. Furthermore, we also formulate our system in terms of two state variables, a and c, which coincide with those used in the original ABM. Hence, we preserve the complexity of the original ABM in Roeder et al. (2006).

The system of equations obtained in this paper is a hyperbolic system of maturity-structured PDEs. Several other maturity-structured models have been formulated, in particular in the context of cell differentiation. For example, Colijn and Mackey (2005) and Pujo-Menjouet and Mackey (2004) provide two age-structured models for normal hematopoiesis and for periodic CML, respectively. In these models, cells spend constant amounts of time in various stages of development before progressing to successive stages. The models are formulated as systems of delay-differential equations (DDEs), where the delay values correspond to the time duration of each cell of the cell development. As an alternative approach, Adimy and Pujo-Menjouet (2003) proposes a model of cell division, in which the duration of each round of proliferation depends on the maturity of the cell. This model is formulated as a system of hyperbolic PDEs with age and maturity variables that both increase over time. The ABM in Roeder et al. (2006) provides, however, an alternative stem cell paradigm that allows stem cells to increase or decrease in affinity over time. Hence, affinity is not a measure of maturity, at least in the conventional sense, but rather of a more generalized state variable. Since stem cells can switch between increasing and decreasing their "maturity" arbitrarily many times, cells do not necessarily mature in finite time. Furthermore, the "left-moving" and "right-moving" populations continually interact and exchange members so that information does not only travel in one direction. These features, inherent in the original formulation of the ABM, reappear in the analogous PDE system presented in this paper.

The paper is organized as follows. We briefly review the Roeder agent-based model in Section 2. A system of PDEs for the emerging cancer dynamics is then derived in Section 3. In this context, we first derive the PDEs that govern the dynamics of the stem cell populations, and pay special attention to the appropriate boundary conditions. We then derive PDEs for normal (nonleukemic) differentiated cells, for leukemia cells and imatinib-affected leukemia cells. In Section 4, we present the results of our numerical simulations. We compare the solutions of the PDE model to the difference equation and the agent-based models by computing steady states of nonleukemia cells, by simulating the CML genesis, and by studying the progression in time of an imatinib treatment. Concluding remarks are provided in Section 5.

2. A brief overview of the Roeder CML model

In this section, we briefly overview the Roeder CML model (Roeder et al., 2006). A state diagram for this model is shown in Fig. 1. In this model, hematopoietic stem cells (HSCs) are assumed to exist in two growth compartments: quiescent (denoted by A) and proliferating (denoted by Ω). At the beginning of every time step (representing one hour), a stem cell may transfer from A to Ω with probability ω or from Ω to A with probability α. Each stem cell has a time-dependent affinity, denoted by $a(t)$, and the affinity ranges between $a_{\min}$ and $a_{\max}$ (which are estimated to be 0.002 and 1.0, respectively (Roeder et al., 2006)).

A cell with a high affinity has a high chance of remaining in the A environment or transferring to it. Likewise, a cell with a low affinity is more likely to remain in the Ω environment or transfer to it, where it starts proliferating. The transition probabilities ω

and α are given by

$$\begin{aligned}\omega\big(\Omega(t), a(t)\big) &= \frac{a_{\min}}{a(t)} f_\omega\big(\Omega(t)\big),\\ \alpha\big(A(t), a(t)\big) &= \frac{a(t)}{a_{\max}} f_\alpha\big(A(t)\big).\end{aligned} \tag{1}$$

Here, $A(t)$ and $\Omega(t)$ denote the total number of cells in each compartment. The functions f_α and f_ω are sigmoidal functions, whose definition can be found in Appendix B.

Proliferating cells in the Ω compartment progress through various stages of the cell cycle: G_1, S, G_2, and M. The G_1 phase is the longest period of growth during which the cell generates new organelles. The S phase is the period when DNA synthesis and replication occurs. The G_2 phase is the short period of growth when the cell prepares for mitosis, and the M phase, or mitosis, is when the cell replicates its DNA and divides into two daughter cells. Only Ω cells in the G_1 phase of the cell cycle can transfer to A. The Ω cells spend about two-thirds of their time in the G_1 phase.

For each cell that remains in the A compartment, its affinity increases by a factor of r (estimated as 1.1). Similarly, cells that remain in Ω, decrease their affinity by a factor of d (estimated as 1.05). The affinity of a cell stops increasing once it reaches the maximal value, $a_{\max}$. Stem cells whose affinity reaches the minimum affinity $a_{\min}$, differentiate into a proliferating precursor and then into a non-proliferating mature cell (see Fig. 1).

Each cell in Ω has an internal time counter, $c(t)$, that indicates its position in the cell cycle (measured in hours). Each time step is equivalent to one hour. Consequently, at each time step, $c(t)$ increases by 1. After $c(t)$ reaches its maximal value of 48, it recycles back to 0 at the next time step, resulting in a 49-hour cell cycle. Cells entering Ω start with a counter that is set at $c(t) = 32$ corresponding to the beginning of the S phase. For the first 17 hours, the cell progresses through the S, G_2, and M phases and divides into two cells once $c(t) = 48$. Then for the next 32 hours, $(c(t) = 0, \ldots, 31)$, the cell remains in the G_1 phase. If at the end of this period the cell has not transferred to A, it reenters the S, G_2, and M phases and the cycle repeats.

The work Roeder et al. (2006) includes an algorithm for simulating the effect of imatinib-treatment on leukemia stem cells. For the sake of brevity, we do not describe the full mechanism here. The complete ABM is summarized in Appendix A.

3. A PDE CML model

3.1. The stem cells

Following Kim et al. (2008), we note that the log of the affinities change linearly in time. We thus index the stem cells with respect to the log of their affinities, by letting $x = -\log a$ where a is the affinity. Then $x \in [x_{\min}, x_{\max}]$, where $x_{\min} = -\log a_{\max}$ and $x_{\max} = -\log a_{\min}$. In our case, we have $x \in [0, 6.2146]$.

Let $A(x,t)$ denote the population density of Alpha cells with $x = \log a$ at time t. As time progresses, the x-components of these cells decrease at a constant rate until they reach $x_{\min}$. At this point, cells start accumulating at the boundary point $x = x_{\min}$.

We thus let $A^*(t)$ denote the population of Alpha cells at the accumulation spot, i.e., the population of cells with minimum log affinity $x = x_{\min}$ (consult Fig. 2).

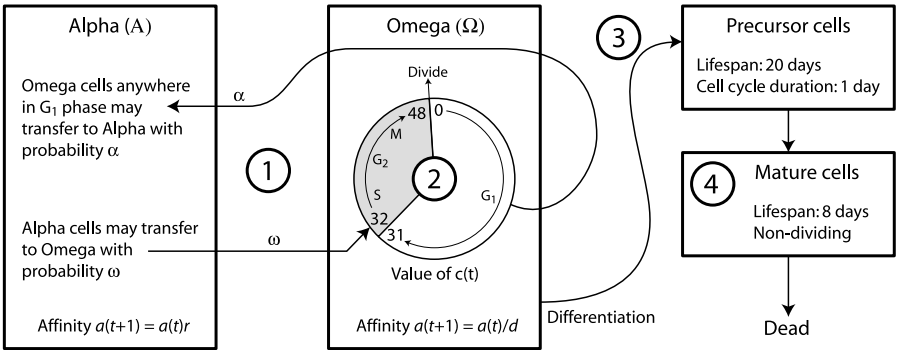

Fig. 1 A state diagram for the Roeder CML model (Roeder et al., 2006). (1) At every time step, stem cells may transfer between the A (nonproliferating) and Ω (proliferating) compartments. While in A, the affinity of each cell increases by a factor of r up to the maximal value, $a_{\max}$. While in Ω, a cell's affinity decreases by a factor of d until it reaches the minimum affinity, $a_{\min}$. (2) Ω cells progress through the G_1, S, G_2, and M phases of the cell cycle. The counter $c(t)$ increases cyclically from 0 to 48. When a cell first enters Ω, $c(t) = 32$ to mark the beginning of S phase. Only cells in the G_1 phase can transfer back to A. (3) When the affinity of a cell drops below $a_{\min}$, it differentiates into a precursor cell. Precursor cells proliferate for 20 days, dividing once per day. (4) At the end of 20 days, precursors differentiate into mature cells and live for 8 additional days without dividing.

For cells in the Omega compartment, let $\Omega(x, c, t)$ denote the population density of these cells with log affinity x and counter c at time t. As time progresses, the x-components of these cells increase at a constant rate, until they reach $x_{\max}$. At the same time, the c-components (that record the position of the cells in their cell cycle) also increase at a constant rate.

There is a continuous supply of cells that are added to the Omega compartment either by transferring from the Alpha compartment or by dividing every 49 hours. As stated in Roeder et al. (2006), cells that transfer from the Alpha compartment, begin with their time counters set to 32. Hence, these cells enter the Omega compartment at the line $c = 32$. In addition, cells that reach a time counter of 49, double and reset their time counters to 0. The cells that transfer into Omega from the A^* state are entering at a point source P and travel along the appropriate characteristic curve with respect to x and c. Let $\Omega^*(x, t)$ denote the population of cells that transferred from A^* into the point source P at time t (see Fig. 2).

We let $\overline{A}$ and $\overline{\Omega}$ denote the total population of cells in the Alpha and Omega compartments, respectively. Then

$$\overline{A}(t) = \int_{x_{\min}}^{x_{\max}} A(x, t)\, dx + A^*(t), \tag{2}$$

$$\overline{\Omega}(t) = \int_{x_{\min}}^{x_{\max}} \int_{0}^{49} \Omega(x, c, t)\, dc\, dx + \int_{x_{\min}}^{x_{\max}} \Omega^*(x, t)\, dx. \tag{3}$$

For the rest of this chapter, we will use the words "Alpha" and "Omega" to refer to the collection of cells in the entire Alpha and Omega compartments, respectively, and we will

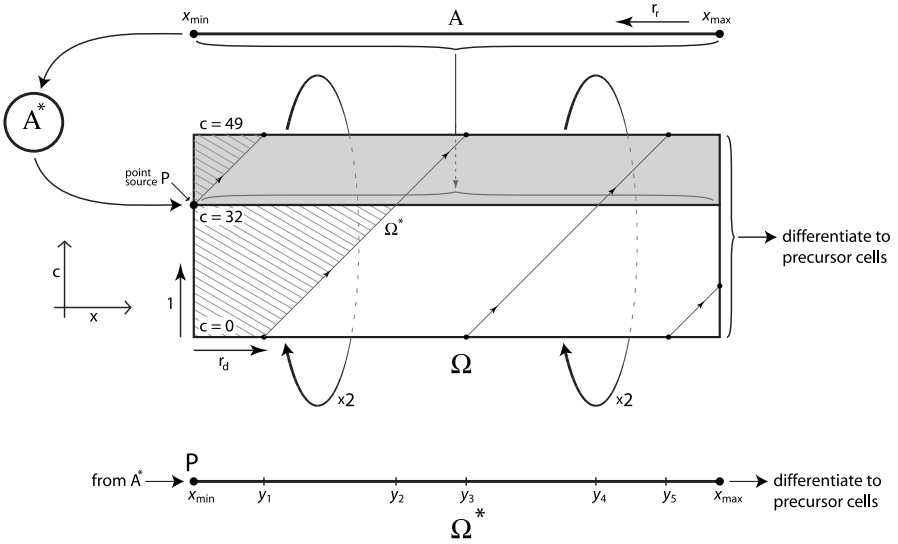

Fig. 2 State space for the PDE CML model. The variable $A(x,t)$ represents cells in the Alpha compartment that have log affinity x at time t. The variable $A^*(t)$ represents cells in the Alpha compartment that have attained the minimum log affinity $x_{\min}$. The variable $\Omega(x,c,t)$ represents the cells in the Omega compartment that have log affinity x and time counter c at time t. The population density $\Omega(x,c,t)$ is always 0 in the striped regions. The shaded region of Ω space between $c=32$ and $c=49$ corresponds to the S, G_2, and M phases of the cell cycle. The unshaded region between $c=0$ and $c=32$ corresponds to the G_1 phase of the cell cycle. The variable $\Omega^*(x,t)$ corresponds to the population of Omega cells supplied by A^*. These cells travel along the characteristic curve originating at point source P. The points y_1, y_2, y_3, y_4, and y_5 correspond to the x-values at which Ω^* cells attain time counters of 49, 32, 49, 32, and 49, after entering the point source P.

use the variable names A, A^*, Ω, and Ω^* to refer to the corresponding subpopulations of the compartments.

We are now ready to formulate the PDEs for each of the populations. For $x \in [x_{\min}, x_{\max})$, A satisfies

$$\frac{\partial A}{\partial t} - \rho_r \frac{\partial A}{\partial x} = -\omega\big(\overline{\Omega}, e^{-x}\big)A + \alpha\big(\overline{A}, e^{-x}\big)\int_0^{32} \Omega(x,c,t)\,dc + \begin{cases} 0, & x \in X_a, \\ \alpha(\overline{A}, e^{-x})\Omega^*, & x \in X_b, \end{cases} \tag{4}$$

where $X_a = (x_{\min}, y_1] \cup (y_2, y_3] \cup (y_4, y_5]$, and $X_b = (y_1, y_2] \cup (y_3, y_4] \cup (y_5, x_{\max}]$. The constants y_1, y_2, y_3, y_4, and y_5 correspond to the values of x at which Ω^* cells attain time counters of 49, 32, 49, 32, and 49, after entering at the point source P. Assuming that $x_{\min} = 0$, the values of y_i are given by

$$y_1 = 17\rho_d, \qquad y_2 = 49\rho_d, \qquad y_3 = 66\rho_d, \qquad y_4 = 98\rho_d, \qquad y_5 = 115\rho_d,$$

where the advection rate ρ_d is given by $\log d$, and d is the differentiation factor estimated as 1.05 in Roeder et al. (2006) (see Table B.1 in Appendix B).

The expression on the LHS of (4) accounts for the linear advection of the A population in the negative x-direction. The advection rate ρ_r is given by $\log r$, where r is the regeneration factor estimated as 1.1 in Roeder et al. (2006).

The first term on the RHS of (4) accounts for the cells that transfer out of A into Ω. The transition rate ω is given by (1), where $\overline{\Omega}$ is defined in (3). The expression e^{-x} recovers the affinity of a cell from its x-coordinate. In the original model, ω is defined as the probability that an individual cell transfers to Omega in a single time step of 1 hour, but if we assume that time is measured in units of hours, this probability ω also gives the transfer rate out of Alpha into Omega.

The second term on the RHS of (4) is the rate in which cells transfer into A from Ω. The transition rate α is given by (1), and $\overline{A}$ is given by (2). Only Ω cells in the G_1 phase (i.e., with time counters c between 0 and 32) can transfer into A, which explains the boundaries in the integral.

The last term on the RHS of (4) is the rate that cells transfer from Ω^* into A. Also in this case, the only cells that can transfer are those with time counters between 0 and 32. As shown in Fig. 2, cells in Ω^* only originate at the point source P and travel at a constant rate along the characteristic curve. Hence, the value of an Ω^* cell's time counter is a function of its x-coordinate. The Ω^* cells that have time counters between 0 and 32 have x-coordinates in the set X_b. Similarly, Ω^* cells that do not have time counters between 0 and 32 have x-coordinates in the complementary set X_a.

For A^*, the following ODE holds:

$$\frac{dA^*}{dt} = \rho_r A(x_{\min}, t) - \omega\big(\overline{\Omega}, e^{-x_{\min}}\big)A^*. \tag{5}$$

The first term on the RHS of (5) is the rate in which cells flow from A into A^*. These A cells flow from the endpoint $x = x_{\min}$ into A^*.

The second term on the RHS of (5) is the rate in which cells flow out of A^* into Ω^*. Cells coming from A^* enter Ω^* at the point source P.

The PDE for Ω is

$$\frac{\partial \Omega}{\partial t} + \rho_d \frac{\partial \Omega}{\partial x} + \frac{\partial \Omega}{\partial c} = \begin{cases} -\alpha(\overline{A}, e^{-x})\Omega, & \text{for } c \in (0, 32], \\ 0, & \text{for } c \in (32, 49]. \end{cases} \tag{6}$$

The second term on the LHS of (6) accounts for the advection of the Ω population in the positive x-direction at rate $\rho_d = \log d$. The third term on the LHS of (6) accounts for the constant rate of increase of the time counter c (the rate is 1). The expressions on the RHS of (6) are the rates that cells transfer out of Ω, depending the values of their time counters. Only cells with time counters between 0 and 32 can leave Ω.

Finally, the PDE for Ω^* is

$$\frac{\partial \Omega^*}{\partial t} + \rho_d \frac{\partial \Omega^*}{\partial x} = \begin{cases} 0, & x \in X_a, \\ -\alpha(\overline{A}, e^{-x})\Omega^*, & x \in X_b. \end{cases} \tag{7}$$

The second term on the LHS of (7) accounts for the constant advection rate of Ω^* cells in the positive x-direction. The RHS of (7) has the rates that cells flow out of Ω^* into A. The RHS is the negative of the last term on the RHS of (4).

3.1.1. Boundary conditions and source terms for stem cells

Any cell in the Omega compartment that has attained the maximal log affinity $x_{\max}$ is destined to differentiate into a precursor cell. Hence, only cells with a smaller log affinity can exist in the Alpha compartment, which means that the boundary condition for A at the endpoint $x = x_{\max}$ is

$$A(x_{\max}, t) = 0. \tag{8}$$

Once Ω cells reach the boundary $c = 49$ they divide, and hence we have

$$\Omega(x, 0, t) = 2\Omega(x, 49, t). \tag{9}$$

At $c = 32$, we have:

$$\Omega\left(x, 32^+, t\right) = \Omega(x, 32^-, t) + \omega\left(\overline{\Omega}, e^{-x}\right)A, \tag{10}$$

where 32^+ and 32^- denote the upper and lower limits as c approaches 32, respectively. The first term on the RHS of (10) is the population of cells already in Ω. The second term on the RHS of (10) corresponds to the rate that cells transfer from A into Ω at $c = 32$. This term is the negative of the first term on the right-hand side of (4). Since the orthogonal rate of advection away from the boundary $c = 32$ is 1, the scaling factor for the second term is also 1.

The boundary condition for Ω^* at the point source P is

$$\Omega^*(x_{\min}, t) = \frac{\omega(\overline{\Omega}, e^{-x_{\min}})}{\rho_d} A^*. \tag{11}$$

This is the rate that cells transfer from A^* into Ω^*, scaled by the advection rate away from P. When the time counters c of the Ω^* cells reach 49, i.e., at y_1, y_3, and y_5, cells divide, and hence we have

$$\Omega\left(y_i^+, t\right) = 2\Omega(y_i^-, t), \quad i = 1, 3, 5. \tag{12}$$

Note that Ω^* is continuous at y_2 and y_4, and hence $\Omega(y_i^+, t) = \Omega(y_i^-, t)$, at $i = 2, 4$.

3.2. The differentiated cells

Once the affinity of a stem cell drops to the minimal value ($\log a(t) \le -127\rho$) or under it, the cell differentiates into a proliferating precursor and later into a nonproliferating mature cell. It then remains in the proliferating precursor state for $\lambda_p = 20$ days (480 hours) and divides every $\tilde{\tau}_c = 24$ hours. At the end of 480 hours, the precursor cell differentiates into a mature cell and lives for $\lambda_m = 8$ additional days (192 hours) without dividing. These durations are given in Roeder et al. (2006) and are summarized in Table B.1. The timeline diagram is shown in Fig. 3.

The PDE for the precursor cells can thus be written as a linear advection equation that represents a simple age-based formulation

$$\frac{\partial P}{\partial t} + \frac{\partial P}{\partial s} = 0, \quad s \in [0, 480). \tag{13}$$

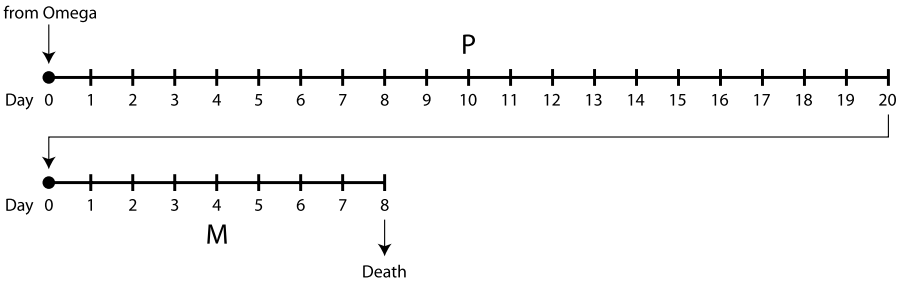

Fig. 3 A time-line diagram for differentiated cells. Precursor cells, P, live for 20 days (480 hours) and divide once per day. Mature cells, M, live for eight days and do not divide.

Here, $P(s,t)$ denotes the population density of precursor cells of age s at time t. Due to cell division, we consider $0, 24, 48, \ldots, 456$, to be "boundary" points. The corresponding boundary conditions are

$$\begin{cases} P(0,t) = \rho_d\left(\int_0^{32} \Omega(x_{\max}, c, t)\, dc + \Omega^*(x_{\max}, t)\right), \\ P(v^+, t) = 2P(v^-, t), \qquad v = 24, 48, 72, \ldots, 456. \end{cases} \tag{14}$$

The expression on the RHS of the first line in (14) is the rate at which Omega cells with minimum affinity flow into precursor state. The second line accounts for cell division of precursor cells every 24 hours.

Similarly, mature cells can be represented by an advection equation

$$\frac{\partial M}{\partial t} + \frac{\partial M}{\partial s} = 0, \quad s \in [0, 192), \tag{15}$$

where $M(s,t)$ is the population density of mature cells of age s at time t. Precursor cells develop into mature cells after completing a final round of division, and hence (15) is augmented by

$$M(0,t) = 2P(480,t). \tag{16}$$

3.3. Leukemia cells and imatinib treatment

We label leukemia cells as Ph^+ and nonleukemia cells as Ph^-. These labels indicate whether or not a cell possesses the Philadelphia chromosome. We formulate a separate set of PDEs for each subpopulation: Ph^- cells, Ph^+ cells, and imatinib-affected Ph^+ cells. These PDEs are similar to (4)–(7), (13), and (15) with few modifications that depend on the specific subpopulation. In all cases, the boundary conditions remain the same as (8)–(12), (14), and (16).

From now on, we define $\overline{A}$ and $\overline{\Omega}$ to denote the total Alpha and Omega populations for all three populations of cells.

We denote the Ph^- populations by A^-, $A^{*,-}$, Ω^-, $\Omega^{*,-}$, P^-, and M^-. The equations for these populations are the original equations (4)–(7), (13), and (15).

We denote the unaffected Ph^+ populations by A^+, $A^{*,+}$, Ω^+, $\Omega^{*,+}$, P^+, and M^+.

These cells are governed by the transition functions, $f_{\alpha/\omega}$, that are defined in terms of the parameters that correspond to unaffected Ph^+ cells in Table B.1. Taking into account these parameters, the populations A^+, $A^{*,+}$, P^+, and M^+ retain the same form as (4), (5), (13), and (15).

On the other hand, proliferating stem cells, Ω^+ and $\Omega^{*,+}$, become imatinib affected at rate r_{inh} and undergo apoptosis at rate $-r_{\text{deg}}$. Let $\alpha^+(\cdot,\cdot)$ denote the transition probability given by (1) that corresponds to unaffected Ph^+ cells. Then Eqs. (6) and (7) are replaced by

$$\begin{aligned}&\frac{\partial \Omega^+}{\partial t} + \rho_d \frac{\partial \Omega^+}{\partial x} + \frac{\partial \Omega^+}{\partial c}\\ &\quad = -(r_{\text{inh}} + r_{\text{deg}})\Omega^+ + \begin{cases} -\alpha^+(\overline{A}, e^{-x})\Omega^+, & c \in (0, 32],\\ 0, & c \in (32, 49],\end{cases}\end{aligned} \tag{17}$$

$$\begin{aligned}&\frac{\partial \Omega^{*,+}}{\partial t} + \rho_d \frac{\partial \Omega^{*,+}}{\partial x}\\ &\quad = -(r_{\text{inh}} + r_{\text{deg}})\Omega^{*,+} + \begin{cases} 0, & x \in X_a,\\ -\alpha^+(\overline{A}, e^{-x})\Omega^{*,+}, & x \in X_b.\end{cases}\end{aligned} \tag{18}$$

Finally, we denote the imatinib-affected Ph^+ populations by A^i, $A^{*,i}$, Ω^i, $\Omega^{*,i}$, P^i, and M^i. These cells are governed by the transition functions, $f_{\alpha/\omega}$ corresponding to imatinib-affected Ph^+ cells in Table B.1. Otherwise as before, the populations A^i, $A^{*,i}$, P^i, and M^i retain the same form as (4), (5), (13), and (15).

In addition, as discussed above, proliferating Ph^+ stem cells become imatinib affected at rate r_{inh}, and imatinib-affected proliferating Ph^+ cells, Ω^i and $\Omega^{*,i}$, also undergo apoptosis at rate r_{deg}. Furthermore, the transition function f_α is the same for both unaffected and imatinib-affected Ph^+ cells, meaning that the transition probability $\alpha^+(\cdot,\cdot)$ also applies to imatinib-affected Ph^+ cells. Hence, the PDEs for Ω^i and $\Omega^{*,i}$ are

$$\begin{aligned}&\frac{\partial \Omega^i}{\partial t} + \rho_d \frac{\partial \Omega^i}{\partial x} + \frac{\partial \Omega^i}{\partial c}\\ &\quad = r_{\text{inh}}\Omega^+ - r_{\text{deg}}\Omega^i + \begin{cases} -\alpha^+(\overline{A}, e^{-x})\Omega^i, & c \in (0, 32],\\ 0, & c \in (32, 49],\end{cases}\end{aligned} \tag{19}$$

$$\begin{aligned}&\frac{\partial \Omega^{*,i}}{\partial t} + \rho_d \frac{\partial \Omega^{*,i}}{\partial x}\\ &\quad = r_{\text{inh}}\Omega^{*,+} - r_{\text{deg}}\Omega^{*,i} + \begin{cases} 0, & x \in X_a,\\ -\alpha^+(\overline{A}, e^{-x})\Omega^{*,i}, & x \in X_b.\end{cases}\end{aligned} \tag{20}$$

We point out that in this model imatinib directly acts on stem cells by causing them to undergo apoptosis and by turning them into imatinib-affected cells, whose transition functions f_α and f_ω are different from those of unaffected cells. In contrast, the model of Michor et al. (2005) assumes that imatinib does not affect stem cells. Instead, in Michor et al. (2005), the effects of imatinib only become apparent at later stages of differentiation.

The terms in (17)–(20) corresponding to coefficients r_{deg} correspond to the rate of apoptosis of Ph^+ stem cells during treatment. The terms in (17)–(20) corresponding to coefficients r_{inh} correspond to the rate that imatinib causes Ph^+ cells to become imatinib-affected.

4. Numerical simulations

4.1. A numerical method

We start by describing the discretization of the equations for the nonleukemia (Ph^-) cells. This system is given by (4)–(7), (13), and (15).

For the stem cells, Eqs. (4)–(7), we divide the domain $[x_{\min}, x_{\max}] \times [0, 49] \times \mathbf{R}_0^+$ into an equally spaced grid. Then the grid points are given by $x_j = j\Delta x$, $c_k = k\Delta c$, and $t_n = n\Delta t$, where $j = 0, \ldots, J$, $k = 0, \ldots, K$, and $n = 0, \ldots, N$. Δx, Δc, and Δt denote the spacings between grid points in the x, c, and t directions, respectively. We let

$$\Delta x = \frac{x_{\max} - x_{\min}}{J} \quad \text{and} \quad \Delta c = \frac{49}{K},$$

and set $\lambda_x = \Delta t/\Delta x$ as the fixed mesh ratio.

We let $\mathcal{T}_u(f)$ denote the composite trapezoidal rule evaluated on the function f with respect to the coordinate u. All integrals that appear in the equations are replaced by a composite trapezoidal rule. Specifically, we let $\mathcal{T}_c(\Omega)$ denote the composite trapezoidal rule approximation for the integral $\int_0^{32} \Omega(x, c, t)\, dc$.

Let $\widehat{A}_n$, $\widehat{\Omega}_n$, $\tilde{A}_{j,n}$, $\tilde{A}^*_n$, $\tilde{\Omega}_{j,k,n}$, and $\tilde{\Omega}^*_{j,n}$ be our numerical approximations for $\overline{A}(t_n)$, $\overline{\Omega}(t_n)$, $A(x_j, t_n)$, $A^*(t_n)$, $\Omega(x_j, c_k, t_n)$, and $\Omega^*(x_j, t_n)$, respectively. Then

$$\widehat{A}_n = \mathcal{T}_x(\tilde{A}_{-,n}) + \tilde{A}^*_n,$$
$$\widehat{\Omega}_n = \mathcal{T}_x \circ \mathcal{T}_c(\tilde{\Omega}_{-,-,n}) + \mathcal{T}_x\big(\tilde{\Omega}^*_{-,n}\big).$$

From (4), we obtain the numerical scheme

$$\begin{aligned}\tilde{A}_{j,n+1} = \tilde{A}_{j,n} &+ \lambda_x \rho_r (\tilde{A}_{j+1,n} - \tilde{A}_{j,n}) \\ &- \Delta t\big(\omega\big(\widehat{\Omega}_n, e^{-x_j}\big)\tilde{A}_{j,n} + \alpha\big(\widehat{A}_n, e^{-x_j}\big)\mathcal{T}_c(\tilde{\Omega}_{j,-,n})\big) \\ &+ \begin{cases} 0, & x_j \in X_a, \\ (\Delta t)\alpha(\widehat{A}_n, e^{-x_j})\tilde{\Omega}^*_{j,n}, & x_j \in X_b. \end{cases}\end{aligned}$$

From (8), we obtain the following boundary condition at $x = x_J$:

$$\tilde{A}_{J,n+1} = 0.$$

Next, we approximate (5) by

$$\tilde{A}^*_{n+1} = \tilde{A}^*_n + \Delta t\big(\rho_r A_{0,n} - \omega\big(\widehat{\Omega}_n, e^{-x_0}\big)\big)\tilde{A}^*_n.$$

Note that $x_0 = 0$ for the parameters in Table B.1.

The equation for Ω cells, (6), is discretized as

$$\tilde{\Omega}_{j,k,n+1} = \tilde{\Omega}_{j,k,n} - \lambda_x \rho_d (\tilde{\Omega}_{j,k,n} - \tilde{\Omega}_{j-1,k,n}) - \lambda_c (\tilde{\Omega}_{j,k,n} - \tilde{\Omega}_{j,k-1,n}) + \begin{cases} -(\Delta t)\alpha(\widehat{A}_n, e^{-x_j})\Omega_{j,k,n}, & \text{for } c \in (0, 32], \\ 0, & \text{for } c \in (32, 49]. \end{cases}$$

On the left edge $x = x_0$, we set

$$\tilde{\Omega}_{0,k,n} = 0, \quad \forall k, n.$$

From (9), for $c = 0$, we have

$$\tilde{\Omega}_{j,0,n+1} = 2\tilde{\Omega}_{j,K,n}.$$

Let $\bar{k}$ be the index between 0 and K such that $c_{\bar{k}}$ is as close to 32 as possible. Then for $c = 32$, we have

$$\tilde{\Omega}_{j,\bar{k}^+,n+1} = \tilde{\Omega}_{j,\bar{k}^-,n+1} + \omega\big(\widehat{\Omega}, e^{-x_j}\big)\tilde{A}_{j,n+1}. \tag{21}$$

Note that (21) implies a jump discontinuity, which occurs at the transition between indices $(j, \bar{k}^-)$ and $(j, \bar{k}^+)$. Similar jump discontinuities occur with Ω^* and P.

The PDE for Ω^*, (7), is discretized as

$$\tilde{\Omega}^*_{j,n+1} = \tilde{\Omega}^*_{j,n} - \lambda_x \rho_d \big(\tilde{\Omega}^*_{j,n} - \tilde{\Omega}^*_{j-1,n}\big) + \begin{cases} 0, & x_j \in X_a, \\ -(\Delta t)\alpha(\widehat{A}, e^{-x_j})\tilde{\Omega}^*_{j,n}, & x_j \in X_b. \end{cases}$$

The boundary condition (11) becomes

$$\tilde{\Omega}^*_{0,n+1} = \frac{\omega(\widehat{\Omega}_n, e^{-x_0})}{\rho_d}\tilde{A}^*_n.$$

For $i = 1$, 3, and 5, let j_i be the index between 0 and J such that x_{j_i} is as close to y_i as possible. Then from (12), for $x = x_{j_1}, x_{j_3}$, and x_{j_5}, we have

$$\tilde{\Omega}^*_{j^+,n+1} = 2\tilde{\Omega}^*_{j^-,n+1}.$$

For the precursor and mature cells, we use the same time discretization as above and divide the age domains $[0, 480]$ and $[0, 192]$ into equally spaced meshes. For simplicity, we choose step sizes of the form $\Delta s = 1/w$, where w is an integer. This way, we can use the same step size for both precursor and mature cells. Hence, the grid points are given by $s_i = i\,\Delta s$ for $i = 1, \ldots, I_m, \ldots, I_p$, where $I_m \Delta s = 192$ and $I_p \Delta s = 480$.

The explicit upwind scheme applied to Eqs. (13), and (15) (for the precursor and the mature cells) reads

$$\tilde{P}_{j,n+1} = \tilde{P}_{j,n} - \lambda_s(\tilde{P}_{j,n} - \tilde{P}_{j-1,n}),$$
$$\tilde{M}_{j,n+1} = \tilde{M}_{j,n} - \lambda_s(\tilde{M}_{j,n} - \tilde{M}_{j-1,n}).$$

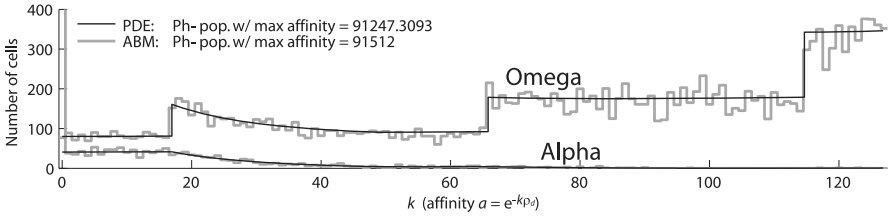

Fig. 4 Steady state profiles for the PDE model and the original agent-based model in the case where there are no leukemia stem cell populations. Cells from the PDE model are plotted with respect to their log affinity values, x. The number is Ph^- cells with maximum affinity is given by A^*. Cells from the Roeder ABM model are grouped into wells based on their log affinity values. The kth well corresponds to cells with affinities between $e^{-(k+1/2)\rho_d}$ and $e^{-(k-1/2)\rho_d}$ for $k = 0, \ldots, 127$. This grouping coincides with what was used in Kim et al. (2008) and allows the ABM data to scale the same way as the solutions of the difference equation model.

Here, $\lambda_s = \Delta t/\Delta s$, and $\tilde{P}$ and $\tilde{M}$ are the numerical approximations for P and M. The boundary conditions are given by

$$\begin{cases} \tilde{P}_{0,n} = \rho_d(\mathcal{T}_c(\tilde{\Omega}_{J,-,n}) + \Omega^*_{J,n}), \\ \tilde{P}_{vw^+,n} = 2\tilde{P}_{vw^-,n}, & \text{for } v = 24, 48, 72, \ldots, 456, \\ \tilde{M}_{0,n} = 2\tilde{P}_{480,n}, \end{cases}$$

where $1/w = \Delta s$ as before.

The discretization of the equations for leukemia cells are derived in the same manner as the scheme for nonleukemia cells. All equations retain the same form, and are omitted for the sake of brevity.

4.2. Nonleukemia cells

Using the scheme from in Section 4.1, we set $\Delta t = 0.1$, $\Delta x = 2\rho_d \Delta t = 0.0098$, and $\Delta c = 0.2$ (which corresponds to $J = 636$ and $K = 245$) and consider the scenario in which there are no leukemia cells. With the parameters in Table B.1 for nonleukemic cells, we obtain the steady state profile shown in Fig. 4 for the Alpha and the Omega stem cells. Omega cells from the PDE model are plotted with respect to their log affinity values, x. Since Ω is a function of both x and c, this variable is integrated with respect to c to obtain the total population of Ω cells with a given log affinity x. Hence, the total Omega population is plotted as

$$\int_0^{49} \Omega(x, c, t_0)\, dc + \Omega^*(x, t_0),$$

where t_0 is fixed.

Figure 4 demonstrates that our new PDE model captures the behavior of the original agent-based model. In the same way, the PDE model agrees closely with the difference equation model of Kim et al. (2008). Figure 5 compares the steady state profiles for nonleukemic cells for the PDE and the difference equation models.

The steady state solution of the PDE model demonstrates that most cells in the Omega compartment originate at the point source P shown in Fig. 2. Specifically, the Ω^* sub-

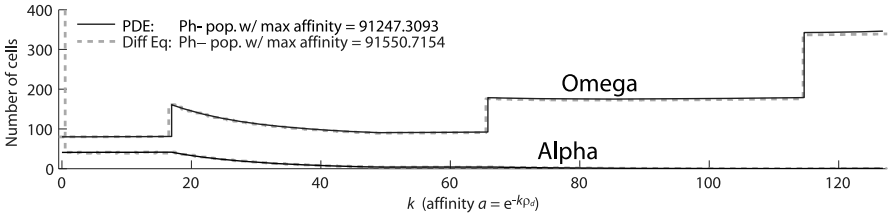

Fig. 5 Steady state profiles for the PDE model and the difference equation model from Kim et al. (2008) in the case where there are no leukemia stem cells.

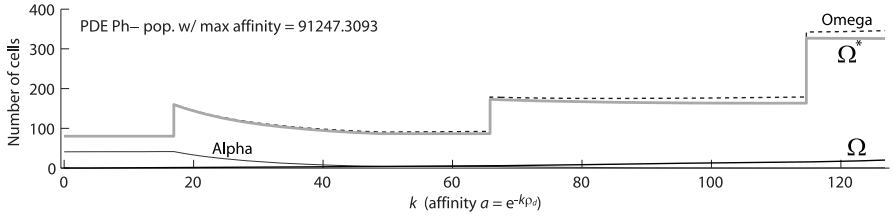

Fig. 6 Steady state profiles for the Omega subpopulations, Ω and Ω^*, of the PDE model.

population accounts for 95% of the total Omega population at steady state. Figure 6 shows the steady state profile of the total Omega population and the Ω^* and Ω subpopulations.

4.3. CML genesis

One of the numerical studies that were conducted in Roeder et al. (2006) was of CML genesis from one leukemia stem cell. The transition from one leukemia cell to a BCR-ABL ratio of over 99%, was captured by simulating the dynamics for up to 15 years.

Such a long time simulation with a PDE model is challenging. We conduct a rather straightforward study by using a coarser mesh that is given by $\Delta t = 0.5$, $\Delta x = 0.0488$, $\Delta c = 1$, and $\Delta s = 0.5$.

Figure 7 shows the results of the numerical simulation of the PDE model. For comparison, they are shown along with simulations of the difference equation model from Kim et al. (2008) and the ABM from Roeder et al. (2006).

From Figure 7, we see that the PDE model captures the same qualitative behavior as the ABM. At the same time, it estimates higher steady state concentrations of Ph^- and Ph^+ cells. On the other hand, the difference equation model from Kim et al. (2008) achieves essentially the same steady state concentrations as the ABM. Hence, it appears that there is a difference between the (continuous time) PDE model and the (discrete time) difference equation and agent-based models.

The steady state solutions of the PDE and of the discrete models have the same qualitative and even structural behavior as shown in Fig. 5. However, from a quantitative perspective, the PDE model estimates higher Alpha and Omega stem cell populations, which in turn result in higher precursor and mature cell populations. Indeed, at the steady state for Ph^- cells, the total numbers of Alpha (dormant) and Omega (proliferating) stem

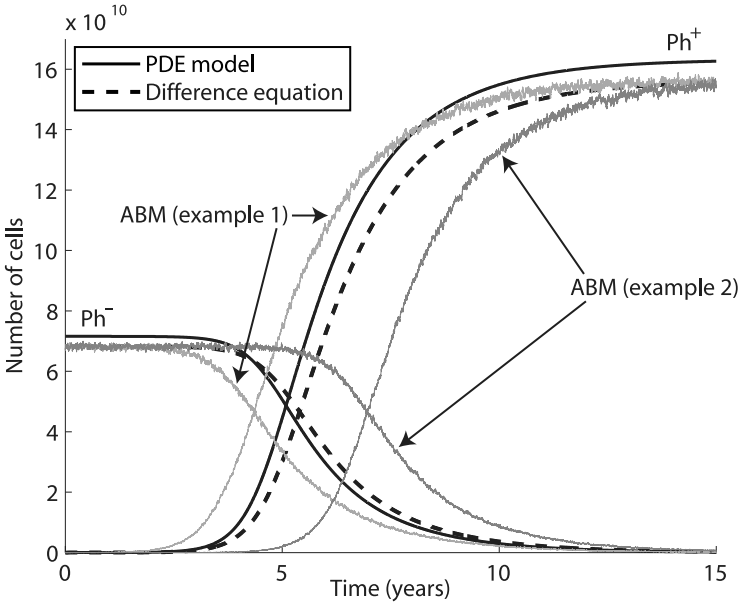

Fig. 7 Simulations of the PDE model and of the difference equation model from Kim et al. (2008). The plot shows the numbers of mature Ph^- and mature Ph^+ cells for both models. The figure also shows two examples of simulations of the ABM from Roeder et al. (2006). The two examples of ABM simulations are the extreme cases out of 100 runs, and most ABM simulations fall between the two examples, closer to the solution given by the difference equation model.

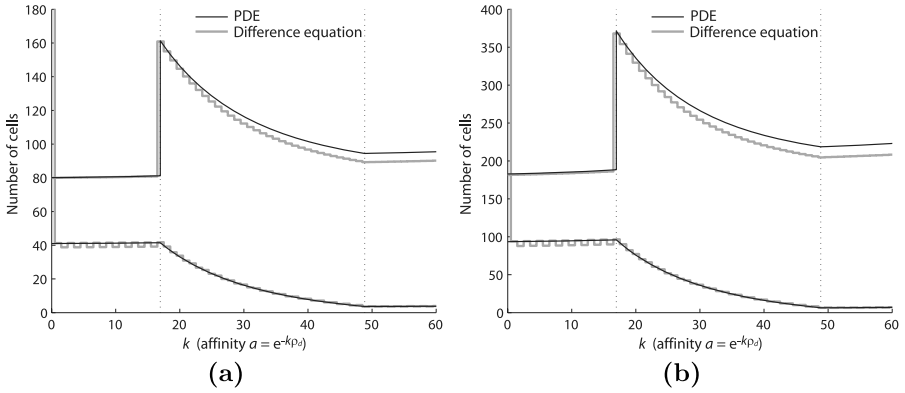

Fig. 8 Comparison between population distributions of stem cells with respect to log(affinity) for the PDE and difference equation models. (a) Ph^- cells. (b) Ph^+ cells after CML genesis.

cells in the PDE model are 9.32×10^4 and 2.00×10^4, whereas for the difference equation model the total numbers of Alpha and Omega stem cells are 9.29×10^4 and 1.94×10^4.

The difference in the way the time variable is handled results in slight differences in accounting for stem cell transitions. These effects accumulate over time, resulting in different quantitative behaviors between the two models. Figure 8 shows an example of how

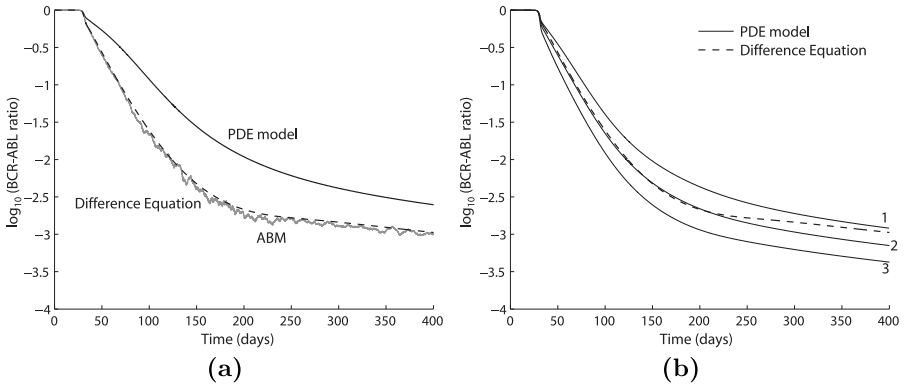

Fig. 9 Time evolution of BCR-ABL ratios under imatinib treatment. The BCR-ABL ratio is defined by (# of mature Ph^+ cells)/((# of mature Ph^+ cells) + 2(# of mature Ph^- cells)) as in Roeder et al. (2006). (a) Plots of the PDE, difference equation, and average of 20 ABM simulations using parameters from Roeder et al. (2006) listed in Appendix B with $r_{\text{inh}} = 0.05$ and $r_{\text{deg}} = 0.033$. As we can see, the difference equation and ABM simulations almost coincide, except that the ABM exhibits some stochasticity, whereas the difference equation model is fully deterministic. (b) Numerical solutions of the PDE model with $(r_{\text{inh}}, r_{\text{deg}})$ values of $(0.1, 0.037)$, $(0.1, 0.04)$, and $(0.1, 0.43)$ for solutions 1, 2, and 3, respectively.

the population distributions of Alpha and Omega cells differ between the PDE and difference equation models. As we notice from the figure, the PDE model does not necessarily average the behavior of the difference equation model. As we see from Figs. 8(a) and 8(b), there are slight differences at every discrete interval along the x-axis of the population distribution. Furthermore, these differences accumulate as x increases, especially for the Omega cells.

4.4. An imatinib treatment

Whereas the differences discussed in Section 4.3 seem relatively minor, the differences between the continuous time and discrete time models become more pronounced in simulations of imatinib treatment. For these simulations. we use the same mesh used in Section 4.3, except that we set $\Delta t = 0.45$ rather than 0.5.

Figure 9(a) compares numerical solutions of the PDE model and the difference equation model using the parameters listed in Appendix B. Figure 9(a) shows how greatly the dynamics vary between the PDE and difference equation models. In particular, the solution to the PDE is much flatter than that of the difference equation model and does not exhibit the bi-phasic decline that was also observed in Roeder et al. (2006). On the other hand, the solutions of the difference equation and agent-based models follow each other very closely (which is not surprising since they are really two equivalent formulations of the same problem).

It is interesting to note that we can obtain the behavior of the difference equation model from the PDE model by increasing the values of r_{inh} and r_{deg} from 0.050 and 0.033 to 0.1 and 0.04, respectively. Figure 9(b) shows three examples of solutions of the PDE model with $(r_{\text{inh}}, r_{\text{deg}})$ values of $(0.1, 0.037)$, $(0.1, 0.04)$, and $(0.1, 0.43)$. Like the difference

equation model, these three examples all exhibit bi-phasic declines that hinge at around 200 days after the start of treatment. Example 2 is especially close to the solution of the difference equation model. We note that in Example 2 the value of r_{inh} is twice as high as the original estimate of 0.050 used in the ABM and the difference equation model. This large difference suggests that the influence of using a continuous-time versus a discrete-time model has a significant effect on the parameter values that cannot be attributed to estimation error alone.

5. Conclusion

In this paper, we derive a CML model that is written as a system of PDEs. This model is a time-continuous extension of the agent-based CML model of Roeder et al. (2006) and of our difference equation model (Kim et al., 2008).

The formulation of a PDE system from the ABM is conceptually challenging due to the assumption that Alpha stem cells increase the affinity until they reach a maximum value, corresponding to the boundary $x = 0$. While this does not pose a problem in the discrete models, in the PDE system, it causes the population density of Alpha cells to accumulate at a point mass at the boundary. Although it may initially appear straightforward to write a simple hyperbolic PDE for Alpha cells and assume that the advection rate remains constant for all $x > 0$ and suddenly becomes 0 at the boundary, this approach leads to various numerical and theoretical difficulties. Various strategies to deal with these problems are discussed in Roeder (2003). As an alternative method in this paper, we separate the population of the point mass at $x = 0$ from the rest of the Alpha stem cell population by introducing a new variable $A^*(t)$. We also introduce a corresponding variable $\Omega^*(x, t)$ for the Omega population. Our expanded system allows for faster numerical evaluation and a natural formulation of the boundary conditions at $x = 0$.[1]

We do not change any of the biological assumptions when deriving the model. The mechanisms that govern the dynamics of the hematopoietic cells remain identical in all models, regardless of whether the cells are leukemic or nonleukemic. The new mathematical formulation, however, is interesting on its own merit. While our PDE model should be considered as a time-continuous limit of both discrete models, the approach we take in deriving this new model is to consider PDEs that are directly based on the biological assumptions. A formal reasoning of this limit is possible, though not particularly instructive.

What are the advantages of a PDE model? In the absence of our previous work (Kim et al., 2008), we could simply claim that the PDE formulation provides a more efficient way of simulating the dynamics (when compared with the agent-based model). In addition, realistic population sizes for the different types of cells can be used. Unlike the agent-based model, the PDE model, has no dependence on the population size.

[1] The numerical evaluation of the PDE model presented in this paper takes a little under 2 hours on our laptop, which is much faster than the ABM model, which takes about 6 hours and 30 minutes on the desktops in the Stanford University Mathematics Department in 2007. On the other hand, the PDE model is still much slower than the difference equation model, which takes about 4 minutes 30 seconds on the desktops (Kim et al., 2008).

In the agent-based case (Roeder et al., 2006), this was a rather strict restriction that limited the sizes of the populations simulated to 10% of their real sizes. These advantages were already noted with our previous work (Kim et al., 2008), and indeed, when compared with that work, our new model, does not improve the efficiency of the simulations.

Nevertheless, the PDE approach has several advantages over the discrete models:

(i) A PDE model provides an alternative representation of the dynamics of the progression of the disease that is continuous in time.
(ii) The PDE approach allows a direct study (and a better fit) of the model parameters that are sensitive to the time being a continuous or a discrete variable.
(iii) The PDE approach allows direct adjustments of global parameters that may depend on macroscopic quantities (such as densities of cells). These are usually less accessible in the discrete models. It also provides direct access to the macroscopic quantities themselves, as the model is formulated in these terms.
(iv) From an implementation point of view, the present model amounts to several (complex) equations. This should be compared with tens of thousands (of rather simple) difference equations in the model of Kim et al. (2008), or with the hundred thousand or so iterations of simple rules at each time step in the ABM of Roeder et al. (2006).

Our numerical simulations demonstrate that the PDE model captures the same qualitative (and structural) behavior of the stem cells in the ABM. Indeed, at equilibrium, most Alpha cells accumulate in the A^* state, representing Alpha cells that have attained maximum affinity. Also, the Omega cells show a step-like behavior with respect to the x-coordinate as shown in Fig. 5. These results coincide with the behavior of the ABM.

The PDE model starts to diverge from the discrete-time (difference equation and agent-based) models when we compare simulations of CML genesis and imatinib treatment. In CML genesis, the PDE model shows the same qualitative behavior as the discrete-time models, but the initial rise of Ph^+ cells occurs earlier, and the Ph^+ cells end at a higher equilibrium concentration than in the discrete-time models.

In simulations of imatinib treatment, the PDE and the discrete-time models diverge more greatly. The results of all models can match if the rates of imatinib-induced inhibition (r_{inh}) and degradation (r_{deg}) are increased. These differences between the ABM and the PDE models demonstrate that some critical aspects of the model are highly sensitive to the discretization of time. This observation is important, because it suggests that it is not straightforward to assume that a discrete-time ABM, albeit with small time steps, accurately approximate the continuous-time behavior.

While it could be argued that a continuous-time description of disease dynamics may be more realistic than discrete-time models, there still are multiple directions in which the present model can be improved, even at the existing resolution (i.e., without adding additional types of cells, signaling, etc.). One example is the deterministic "clock" that governs the progression of cells in the Omega state, the deterministic nature of the affinity variable, or the deterministic life-cycle of precursor cells. These could be ideal places to add some uncertainty the model, an issue we plan to address in the future.

Appendix A: The ABM algorithm

We summarize the algorithm of the ABM from Roeder et al. (2006).

At every time step, the ABM is defined as the following set of actions:

A. Preliminary calculations

1. Calculate the total populations of A and Ω cells.
2. During imatinib treatment:
   - Remove the proliferative Ph^+ cells (Ω^+ and $\Omega^{+/i}$) that undergo apoptosis.
   - Determine which unaffected proliferative Ph^+, Ω^+, become imatinib-affected.

B. Proliferation, death, change of state, clocks

At this stage, all cells fall into one of three categories: A stem cells, Ω stem cells, differentiated cells.

1. For each A stem cell:
   - Determine whether the cell transfers to Ω. If a cell transfers, skip the remaining actions for A cells. Note that the transition function depends on whether the cell is Ph^-, Ph^+, or imatinib-affected. Calculate transition probabilities based on the total population of Ω calculated in Step A1.
   - Increase the cell's affinity by a factor of r.
2. For each Ω stem cell:
   - Determine whether the cell transfers to A. If a cell transfers, skip the remaining actions for Ω cells. Calculate transition probabilities based on the total population of A calculated in Step A1.
   - If the cell's affinity is less than or equal to $a_{\min}$, the cell becomes a differentiated cell of age 0. If the cell differentiates, skip the remaining actions for Ω cells.
   - If a cell's affinity is greater than $a_{\min}$, decrease the cell's affinity by a factor of d.
   - Increase the counter c by 1.
   - If the counter c is greater than or equal to 49, set c to 0 and create a new cell with identical attributes and state values as the current cell.
3. For each differentiated cell:
   - Increase the cell's age by one.
   - If the cell's age is a multiple of 24 between 24 and 480, inclusively, create a new differentiated cell with the same age as the current cell.
   - If a cells age reaches 672, that cell dies.

Table B.1 Parameters from Roeder et al. (2006)

Parameter	Description	Ph^-	Ph^+/imatinib-affected
$a_{\min}$	Min value of affinity a	0.002	0.002
$a_{\max}$	Max value of affinity a	1.0	1.0
d	Differentiation coefficient	1.05	1.05
r	Regeneration coefficient	1.1	1.1
τ_c	Cell cycle duration	48 hours	48 hours
τ_S	Duration of S phase	8 hours	8 hours
$\tau_{G_2/M}$	Duration of G_2 and M phases	8 hours	8 hours
λ_p	Lifespan of proliferating precursor cells	20 days	20 days
λ_m	Lifespan of mature cells	8 days	8 days
$\tilde{\tau}_c$	Cell cycle of proliferating precursors	24 hours	24 hours
$f_\alpha(0)$	Transition characteristic for f_α	0.5	1.0
$f_\alpha(\tilde{N}_A/2)$	Transition characteristic for f_α	0.45	0.9
$f_\alpha(\tilde{N}_A)$	Transition characteristic for f_α	0.05	0.058
$f_\alpha(\infty)$	Transition characteristic for f_α	0.0	0.0
$\tilde{N}_A$	Scaling factor	10^5	10^5
$f_\omega(0)$	Transition characteristic for f_ω	0.5	1.0/0.0500
$f_\omega(\tilde{N}_A/2)$	Transition characteristic for f_ω	0.3	0.99/0.0499
$f_\omega(\tilde{N}_A)$	Transition characteristic for f_ω	0.1	0.98/0.0498
$f_\omega(\infty)$	Transition characteristic for f_ω	0.0	0.96/0.0496
$\tilde{N}_A$	Scaling factor	10^5	10^5

Note that differentiated cells of age less than 480 are considered to be proliferating precursors, whereas differentiated cells of age greater than or equal to 480 are considered to be non-proliferating mature cells.

Appendix B: Parameter estimates

The sigmoidal transition functions are given in Roeder et al. (2006) by

$$f_{\alpha/\omega}(\overline{A}/\overline{\Omega}) = \frac{1}{\nu_1 + \nu_2 \exp\left(\nu_3 \frac{\overline{A}/\overline{\Omega}}{\tilde{N}_{A/\Omega}}\right)} + \nu_4, \tag{B.1}$$

where $\overline{A}$ and $\overline{\Omega}$ denote the total populations in the Alpha and Omega compartments, respectively (see (2) and (3)). Furthermore,

$$\nu_1 = \left(h_1 h_3 - h_2^2\right)/(h_1 + h_3 - 2h_2),$$
$$\nu_2 = h_1 - \nu_1,$$
$$\nu_3 = \ln(h_3 - \nu_1/\nu_2),$$
$$\nu_4 = f_{\alpha/\omega}(\infty),$$

Table B.2 Imatinib-related parameters from Roeder et al. (2006). The inhibition intensity, r_{inh}, refers to the probability that a proliferative Ph^+ cell (i.e., an Ω cell) becomes imatinib-affected in a given time interval. The degradation intensity, r_{deg}, refers to the probability that an imatinib-affected, proliferative Ph^+ cell dies in a given interval

Parameter	Description	Estimate
r_{inh}	Inhibition intensity	0.050
r_{deg}	Degradation intensity	0.033

and

$$h_1 = \left(f_{\alpha/\omega}(0) - f_{\alpha/\omega}(\infty)\right)^{-1},$$
$$h_2 = \left(f_{\alpha/\omega}(\tilde{N}_{A/\Omega}/2) - f_{\alpha/\omega}(\infty)\right)^{-1},$$
$$h_3 = \left(f_{\alpha/\omega}(\tilde{N}_{A/\Omega}) - f_{\alpha/\omega}(\infty)\right)^{-1}.$$

The values of the various parameters are listed in Table B.1.

Acknowledgements

This work was supported by a Research Scholar Award from the American Cancer Society to PPL. The work of DL was supported in part by the NSF under Career Grant DMS-0133511. The work of PSK was supported in part by the Chateaubriand fellowship.

References

Abbott, L.H., Michor, F., 2006. Mathematical models of targeted cancer therapy. Br. J. Cancer. 95(9), 1136–1141.

Adimy, M., Pujo-Menjouet, L., 2003. A mathematical model describing cellular division with a proliferating phase duration depending on the maturity of cells. Electron. J. Differ. Equ. 2003(107), 1–14.

Campbell, J.D., Cook, G., Holyoake, T.L., 2001. Evolution of bone marrow transplantation—the original immunotherapy. Trends Immunol. 22(2), 88–92.

Colijn, C., Mackey, M.C., 2005. A mathematical model of hematopoiesis–I. Periodic chronic myelogenous leukemia. J. Theor. Biol. 237(2), 117–132.

DeConde, R., Kim, P.S., Levy, D., Lee, P.P., 2005. Post-transplantation dynamics of the immune response to chronic myelogenous leukemia. J. Theor. Biol. 236(1), 39–59.

Dingli, D., Michor, F., 2006. Successful therapy must eradicate cancer stem cells. Stem Cells 24(12), 2603–2610.

Druker, B.J., Lydon, N.B., 2000. Lessons learned from the development of an ABL tyrosine kinase inhibitor for chronic myelogenous leukemia. J. Clin. Invest. 105(1), 3–7.

Fokas, A.S., Keller, J.B., Clarkson, B.D., 1991. Mathematical model of granulocytopoiesis and chronic myelogenous leukemia. Cancer Res. 51(8), 2084–2091.

Kim, P.S., Lee, P.P., Levy, D., 2007. Mini-Transplants for Chronic Myelogenous Leukemia: A Modeling Perspective. In: Queinnec et al. (Eds.), Biology and Control Theory: Current Challenges, Lecture Notes in Control and Information Sciences, vol. 357, pp. 3–20.

Kim, P.S., Lee, P.P., Levy, D., 2008. Modeling imatinib-treated chronic myelogenous leukemia: reducing the complexity of agent-based models. Bull. Math. Biol. 70(3), 728–744.

Komarova, N.L., Wodarz, D., 2005. Drug resistance in cancer: Principles of emergence and prevention. Proc. Natl. Acad. Sci. USA 102(27), 9714–9719.

Michor, F., Hughes, T.P., Iwasa, Y., Branford, S., Shah, N.P., Sawyers, C.L., Nowak, M.A., 2005. Dynamics of chronic myeloid leukaemia. Nature 435, 1267–1270.

Moore, H., Li, N.K., 2004. A mathematical model for chronic myelogenous leukemia (CML) and T cell interaction. J. Theor. Biol. 225(4), 513–523.

Neiman, B., 2002. A mathematical model of chronic myelogenous leukemia. Master's thesis, University College, Oxford University, UK.

Pujo-Menjouet, L., Mackey, M.C., 2004. Contribution to the study of periodic chronic myelogenous leukemia. C. R. Biol. 327, 235–244.

Roeder, I., 2003. Dynamical modeling of hematopoietic stem cell organization—Design and validation of the new concept of within-tissue plasticity. PhD thesis, University of Leipzig, Germany.

Roeder, I., Glauche, I., 2008. Pathogenesis, treatment effects, and resistance dynamics in chronic myeloid leukemia—insights from mathematical model analyses. J. Mol. Med. 85(1), 17–27.

Roeder, I., Horn, M., Glauche, I., Hochhaus, A., Mueller, M.C., Loeffler, M., 2006. Dynamic modeling of imatinib-treated chronic myeloid leukemia: functional insights and clinical implications. Nat. Med. 12(10), 1181–1184.

Thijsen, S.F.T., Schuurhuis, G.J., van Oostveen, J.W., Ossenkoppele, G.J., 1999. Chronic mlyeloid leukemia from basics to bedside. Leukemia 13(11), 1646–1674.